

Colour Image Segmentation by the Vector-valued Allen-Cahn Phase-field Model: a Multigrid Solution

David A Kay * Alessandro Tomasi

Abstract

We propose a new method for the numerical solution of a PDE-driven model for colour image segmentation and give numerical examples of the results. The method combines the vector-valued Allen-Cahn phase field equation with initial data fitting terms. This method is known to be closely related to the Mumford-Shah problem and the level set segmentation by Chan and Vese. Our numerical solution is performed using a multigrid splitting of a finite element space, thereby producing an efficient and robust method for the segmentation of large images.

This work has been submitted to the IEEE for possible publication. Copyright may be transferred without notice, after which this version may no longer be accessible.

I. INTRODUCTION

The Mumford-Shah functional was first proposed in [24] as a general way to pose the problem of image segmentation. Reviews can be found for example in Petitot [26], and Fusco [12]. The generality of its statement has led to several methods of solution; in particular, the model sometimes referred to as the reduced Mumford-Shah was solved by the level set method by Chan and Vese [8], based on a previous paper on the motion of multiphase junctions tracked by the level set method by Zhao, Chan, Merriman and Osher [33], and subsequently extended in Chan and Vese [6], [7], [9], Vese [29], Chan, Shen and Vese [5]. Due to the extent of their work, it is also often referred to as the Chan-Vese model. The level set is used to track the boundaries of objects and should converge to the set of contours in the image.

Esedoğlu and Tsai [11] proposed the Allen-Cahn equation, also known as the phase field model, as a method of solution to the reduced Mumford-Shah problem when used in conjunction with the Chan-Vese fitting terms. The Allen-Cahn equation has been used in the context of image processing by Beneš, Chalupecký and Mikula [3], who first convolve the image with a Gaussian smoothing kernel to eliminate noise, and then use it as an anisotropic gradient filter based on the proposals by Perona and Malik [20]. Our approach differs significantly in that we use no smoothing kernel and we modify the energy functional by adding fitting terms; moreover, we use the vector-valued formulation of the Allen-Cahn equation due to Garcke, Nestler and Stoth [13].

A different phase transition model (Modica-Mortola) was also recently used by Jung, Kang and Shen [14], and although the model and numerical method of solution therein differs from this work, it is in many ways similar in the fundamental approach of adapting a phase transition model to solve the Mumford-Shah problem, and in the results obtained.

Oxford Computing Laboratory, Wolfson Building, Parks Road, Oxford, OX1 3QD, UK.
David.Kay@comlab.ox.ac.uk Tel: 0044 (0)1865 610814

Department of Mathematics, University of Sussex, Falmer, Brighton, BN1 9RF, UK. keug1@sussex.ac.uk Tel: 0044 (0)1273 873450. Corresponding author.

Our computations are solved by a multigrid algorithm which falls into the category of Successive Subspace Corrections (see Xu [30], [31]). This was successfully applied to the vector-valued Allen-Cahn equation in Kornhuber, [17], Kornhuber and Krause [18], [19] with a small variation (see Kornhuber and Krause [15]).

In section II we briefly introduce and summarise previous directly relevant work leading up to section II-C, in which we formally introduce our own formulation and show how the minimisation of our functional leads to the desired system of PDEs; in section III we discretise the system and introduce the numerical method of solution, and in section IV we present a few practical aspects of implementation together with examples.

II. IMAGE SEGMENTATION BY THE ALLEN-CAHN EQUATION

A. Relation to the Mumford-Shah functional

Given an image $I \in \Omega \subset \mathbb{R}^2$, the Mumford-Shah method seeks to partition the domain Ω into several subdomains Ω_i separated by a set K of boundaries, also known as edges or discontinuities. This segmentation takes the form of piecewise smooth functions $u \in \Omega - K$ which are discontinuous on K ; the method of selection from all possible functions u is minimisation of an energy functional

$$MS(u) = \int_{\Omega-K} |\nabla u|^2 dx + \mu \int_K d\sigma + \lambda \int_{\Omega} (u - I)^2 dx \quad (1)$$

where μ, λ are positive constants.

The first term minimises the variation of u and promotes its smoothness, the second term minimises the length of interfaces and determines the boundaries between Ω_i , and the third term, sometimes referred to as the fidelity or fitting term, minimises the variation between u and I .

As noted in Petitot [26], the coefficients μ and λ define several scales of the problem: low μ leads to fine-grain segmentation, high μ to coarse-grain results. Sensitivity to contrast is measured by $(4\lambda^2\mu)^{1/4}$ and robustness to noise depends on $\lambda\mu$.

Many variations on this theme have been proposed since its first formulation. Mumford and Shah themselves pointed out that a reduced form of the problem, referred to as the minimal partition problem, is the restriction of u to piecewise constant functions, i.e. $u = c_i$ with each c_i a constant on each connected region Ω_i . The minimising values are then clearly the averages of I across each region.

In the level set case, using by way of example a single function ϕ to segment an image containing only one object against a background, the Chan-Vese functional introduced in [8] replaces the fidelity term in $MS(u)$ by two fitting terms,

$$F_1(\phi) + F_2(\phi) = \int_{\text{inside}(\phi=0)} |I - c_1|^2 dx + \int_{\text{outside}(\phi=0)} |I - c_2|^2 dx \quad (2)$$

where c_1, c_2 are the average of I inside and outside $\phi = 0$, respectively. Considering for a moment the ideal situation in which the image contains only one object, i.e. is split into two regions of roughly constant value clearly separated by a gradient boundary, these two terms are clearly minimised when the set $\phi = 0$ coincides with the contour of the object, i.e. the set K .

B. A phase-field formulation

The Allen-Cahn PDE was introduced in [1] to model the domain coarsening occurring after a phase transition. It follows the evolution of a function $u(x)$ known as the *order parameter*, which smoothly varies between the values of 0 and 1 across an interface¹ to represent which parts of the

¹The original model was defined on the interval $[-1,1]$, but it is convenient to consider $[0,1]$ for our purposes, without loss of generality.

material are in one phase or another. It is obtained by minimising the following energy functional:

$$AC(u) = \int_{\Omega} \epsilon |\nabla u|^2 + \frac{1}{4\epsilon} \Psi(u) \, dx \quad (3)$$

The function $\Psi(u)$ represents a potential that attains minimal values at the two extreme values of u . This is not in general a convex function, nor is it necessarily smooth. Esedoğlu and Tsai [11], for example, chose the quartic double-well form of the potential, $\Psi(u) = u^2(1-u)^2$.

Comparing the first two terms in (1) and (3), the first term is identical up to a scaling constant, while the role of the second term is quite similar since the parameter ϵ is directly related to the width of interfaces between phases; it is well known that minimising $\Psi(u)$ as above reduces both the width and length of boundaries. In this paper, we examine the results of extending (3) to its vector-valued formulation and combining it with fitting terms such as those in (2).

It is reasonable to suggest that the results obtained by a level set method and a phase-field method should be closely comparable because both are known to be equivalent to curve motion by mean curvature; for an overview, see for example [10].

The method of solution described in [11] follows the MBO thresholding scheme by Merriman, Bence and Osher [21], [22], which assigns to the order parameter either one or the other extremal value at each step; we propose to use the formulation known as the *double obstacle* instead, in which, Ψ takes the form

$$\Psi(u) = \Phi(u) + Q(u),$$

where

$$\Phi(u) = \begin{cases} 0 & u \in [0, 1] \\ +\infty & u \notin [0, 1] \end{cases}$$

is known as the *indicator function* on the set $[0, 1]$, and $Q(u)$ is the concave quadratic

$$Q(u) = u(1-u).$$

C. A modified vector-valued Allen-Cahn equation

Our primary objective is to achieve a fast, robust image segmentation method. Given a domain $\Omega \subset \mathbb{R}^2$ and an image $I: \Omega \rightarrow \mathbb{R}^c$ with c data channels or colours, we follow the motion of a function u with several (N) components that we want to adapt to the significant features of I . We propose to do this by solving a system of PDEs on a finite-element space by a multigrid method, and we derive this system by minimising an energy functional of the form

$$\mathcal{E} = \int_{\Omega} \epsilon \frac{|\nabla u|^2}{2} + \frac{u(1-u)}{\epsilon} + \Phi(u) + \lambda u \cdot F(c, I) \, dx, \quad (4)$$

where

$$F(c, I) = (I - c)^2, \quad c = \frac{\int_{\Omega} uI}{\int_{\Omega} u}, \quad (5)$$

the quantity c representing the average of I in u , in other words being a measure of the oscillation of the data over the support of u .

In order to achieve a simultaneous segmentation of I into arbitrarily many pieces, we refer to the vector-valued formulation of the Allen-Cahn system was introduced in Garcke, Nestler and Stoth

[13], which allows one to consider an arbitrary number of components to the order parameter, now described by a single vector-valued function $u \in \mathcal{V}^N$ in the function set defined as

$$\mathcal{V}^N := \left\{ v \in (H^2(\Omega))^N : \sum_{i=1}^N v_i(x) = 1 \text{ a.e. in } \Omega, \quad v_i \geq 0 \text{ a.e. in } \Omega \right\}, \quad (6)$$

In other words, the vector-valued function u must pointwise remain on the N -dimensional Gibbs Simplex

$$\mathbb{G}^N := \left\{ x \in \mathbb{R}^N \left| \sum_{i=1}^N x_i = 1, \quad 0 \leq x_i \right. \right\}, \quad (7)$$

which is itself an $(N - 1)$ -dimensional subset of the hyperplane

$$\Sigma^N := \left\{ x \in \mathbb{R}^N \left| \sum_{i=1}^N x_i = 1 \right. \right\}.$$

Trivially, $x_i \leq 1 \forall x \in \mathbb{G}^N$ (though not so for all $x \in \Sigma^N$).

An N -dimensional extension to the potential function $\Psi(u)$ is now required, with N minima given by $u_j = 1, u_{i \neq j} = 0$; the form

$$Q(u) = \sum_{i=1}^N u_i(1 - u_i)$$

has been used in the following, with $\Phi(u)$ now the indicator function on \mathbb{G}^N and $\Psi(u) = \Phi(u) + Q(u)$ as for the standard double-obstacle Allen-Cahn.

Following standard procedure, we wish to minimise the energy functional (4) to derive a pde to which we can introduce a pseudo-time stepping to find a global minimum. To find the variational derivative of (4) in a direction v , care must be taken to remain in \mathbb{G}^N ; in other words, we do not want our function to leave the allowed set. If considering $\mathcal{E}(u + \alpha v)$ for some $\alpha \in \mathbb{R}$, it must be that $\sum_i u + \alpha v = \sum_i u = 1$, and hence $\sum_i \alpha v = 0$. To that end, Garcke, Nestler and Stoth [13] introduce the hyperplane

$$T\Sigma^N := \left\{ u \in \mathbb{R}^N \left| \sum_{i=1}^N u_i = 0 \right. \right\}$$

which is at all points tangent to Σ^N (and hence to \mathbb{G}^N), together with the projection operator T defined by

$$Tx := x - \frac{1}{N}(x \cdot 1_N) \cdot 1_N \quad (8)$$

as acting on a vector $x \in \mathbb{R}^N$, where $1_N := (1, 1 \dots 1) \in \mathbb{R}^N$. Geometrically, the two hyperplanes Σ^N and $T\Sigma^N$ are parallel; $T\Sigma^N$ passes through the origin; the vector

$$\hat{N} := \frac{1_N}{N} \in \mathbb{G}^N$$

is normal to $T\Sigma^N$ and represents the shortest distance between Σ^N and $T\Sigma^N$. As N grows larger, this distance grows smaller. By construction, $u - v \in T\Sigma^N \forall u, v \in \Sigma^N$.

We now turn to the question of minimising (4). As is usual for the Allen-Cahn functional (3), we use a gradient descent method, i.e. we find the directional derivative of (4), and obtain a variational inequality to be solved numerically. Using the notation $\langle \cdot, \cdot \rangle$ to indicate the standard inner product, and using the the N -subgradient

$$\partial\Phi(u) := \left\{ \xi \in \mathbb{R}^N \mid \Phi(v) - \Phi(u) \geq \xi(v - u) \right\},$$

since we have

$$\langle \xi, u - v \rangle \geq 0 \quad \forall u, v \in \text{dom } \Phi, \forall \xi \in \partial\Phi(u). \quad (9)$$

it is easy to see that a simple minimisation with respect to the order parameter u , which subsequently determines the constants c_i as well (as seen in [8]), leads to

$$\left\langle \frac{\partial}{\partial u} \mathcal{E}(u), Tv \right\rangle \geq \left\langle -\epsilon \Delta u - \frac{2}{\epsilon} u + \lambda F(c, I) + \frac{1}{\epsilon} \xi, Tv \right\rangle$$

and hence, by introducing a pseudo-time parametrisation, we have the inclusion

$$\langle u_t - \epsilon \Delta u + T \left(-\frac{2}{\epsilon} u + \lambda F(c, I) \right), v - u \rangle \ni \langle -\partial\Phi(u), v - u \rangle \quad (10)$$

$$\geq 0 \quad (11)$$

$\forall u, v \in \mathcal{V}^N$. An approximation to this variational inequality can naturally be sought in terms of a finite element method, as described below.

III. DISCRETISATION AND NUMERICAL SOLUTION

It has been shown that iterative solvers such as the Jacobi, Gauss-Seidel, Successive Over-Relaxation and multigrid methods can be reduced to a class known as *Subspace Correction* methods; these first appeared in Xu [30], see also Xu [31], Kornhuber [16]. Convergence of subspace correction methods has been examined for example in Tai and Xu [27] for convex optimisation problems and in Neuss [25].

In essence, it is shown that a viable alternative to constantly projecting the solution from one level to another is to once and for all project all basis functions from all multigrid levels onto the coarsest one, solving the problem by iterating through all basis functions. An example of this projection method is shown in figure 2. This method was successfully applied to the vector-valued Allen-Cahn equation by Kornhuber [17], Kornhuber and Krause [18], [19].

In subsection III-A we introduce the finite element method to establish the notation; building upon that basis, subsection III-B shows the multigrid discretisation used, while subsection III-C details a few aspects of the numerical implementation due to the Gibbs Space constraint and the double-obstacle method.

A. Finite Element Notation

The continuous domain Ω is split into a set of subdomains \mathcal{T} , referred to as a *triangulation*, given by the set of triangles τ such that

$$\bar{\Omega} = \bigcup_{\tau \in \mathcal{T}} \bar{\tau}$$

The natural length scale associated with each triangulation is

$$h := \max_{\tau \in \mathcal{T}} \text{diam}(\tau).$$

The vertices of all triangles form a set of n points or *nodes*, and for the purposes of this work, each triangulation is further required not to have any *hanging nodes*, i.e. nodes that are not corners of a triangle. Each node $x_i \in \Omega$, $i = 1 \dots n$ is assigned a function $\eta_i(x)$ such that

$$\eta_i := \begin{cases} 1 & \text{if } x = x_i; \\ 0 & \text{if } x \neq x_i. \end{cases}$$

Although these functions can be arbitrarily elaborate while still satisfying the specified requirements, continuous piecewise linear functions are more than adequate for second-order problems such as ours. The set of all such functions, which can also be written as

$$\mathcal{S} := \left\{ \eta \in C(\overline{\Omega}) : \eta|_{\tau} \text{ is linear } \forall \tau \in \mathcal{T} \right\}, \quad (12)$$

forms a basis for the finite element space

$$\mathcal{V}^h = \text{span} \{ \eta_i \}_{i=1}^n \quad (13)$$

such that all functions $u^h \in \mathcal{V}^h$ can be represented as

$$u^h(x) = \sum_{i=1}^n u_i^h \eta_i(x) \quad (14)$$

and such that continuous functions u on the original domain can be represented on the triangulation by their piecewise linear interpolant $\pi: C(\overline{\Omega}) \rightarrow \mathcal{V}^h$.

We use the lumped mass and stiffness matrices

$$\hat{M} := \sum_{j=1}^n M = \langle \eta_i, 1 \rangle, \quad A := \langle \nabla \eta_i, \nabla \eta_j \rangle \quad \forall \eta_i, \eta_j \in \mathcal{V}^h.$$

To discretise the inequality in (11) by the finite element method, we pass to the the weak formulation

$$\left\langle u_i^h + T \left(-\frac{2}{\epsilon} u^h + \lambda F(c, I) \right), v^h - u^h \right\rangle - \epsilon \langle \nabla u^h, \nabla (v^h - u^h) \rangle \geq 0 \quad \forall v^h \in \mathcal{V}^h \quad (15)$$

so that the discrete solution u^h is only required to have H^1 regularity. We can then consider the above problem as a series of sub-problems over each basis function. This is known to be equivalent to an iterative solver, such as a Gauss-Seidel method; the precise sequence in which these are considered can be altered for instance to follow a red-black Gauss-Seidel pattern. By simple application of the properties of the projection operator T , using the discretisation method outlined above, we have n problems of the form

$$\left(u_i + T \left(-\frac{2}{\epsilon} u + \lambda F(c, I) \right) \right) \hat{M}(v - u) - \epsilon u A(v - u) \geq 0. \quad (16)$$

with some appropriate time discretisation to follow. The inequality is due to the multi-valued nature of the subgradient at the boundaries of \mathbb{G}^N ; each iteration in the numerical method is performed as though (16) were a strict equality, and if the result lies outside the acceptable space, then it is projected appropriately, as described in section III-C.

B. Multigrid Solution

The rate of convergence of Gauss-Seidel methods requires $O(n)$ iterations per time-step, and $O(n^2)$ computations overall to converge to a solution, which is less than optimal. Multigrid methods are known to be more efficient, in most cases being of only $O(n)$ complexity overall; they rely on constructing several nested finite element spaces, usually by refining a *coarse* or *macro* triangulation \mathcal{T}_1 $L - 1$ times, eventually giving the *fine* triangulation \mathcal{T}_L , where

$$\mathcal{T}_l \subset \mathcal{T}_{l+1}.$$

Figure 1 shows a simple example of one such refinement. Each triangulation is associated with its own finite element function space. Using projection and restriction operators, the solution is

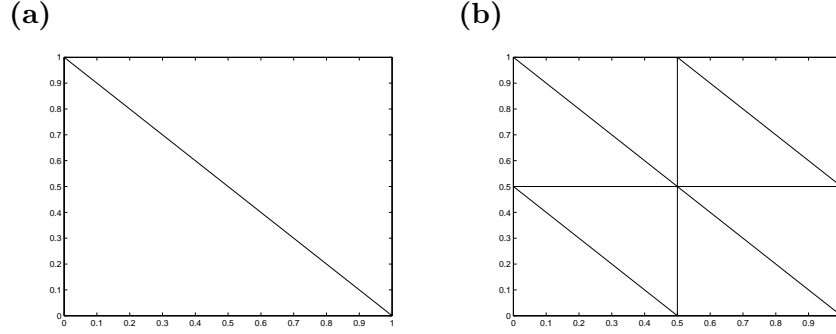


Fig. 1. a) A coarse grid; b) the same grid, after one refinement.

computed on one level, usually by a Gauss-Seidel solver or equivalent, and then passed to another level to be corrected. The theoretical basis of the multigrid method lies in showing that the error at each iteration can be considered to have several components of varying frequency, and that each time the problem is solved on a grid of natural spacing h , the error components that are of frequency h or higher are all reduced significantly, while those with a lower frequency are barely affected. The multigrid method significantly improves convergence by using several levels to deal with many components of the error in every iteration.

A recent development in multigrid methods has been to consider iterative solvers as part of the *Successive Subspace Correction* framework, which simply considers a minimisation over a sequence of function spaces such as (13), each defined as the set spanned by the basis functions defined on a different grid. In the context of finite elements, such a hierarchy of function sets is readily provided by the basis functions at each level of refinement. To be more precise, given the problem $\mathcal{P}_{i,j}$: find u such that

$$\langle u_i^h + T\left(-\frac{2}{\epsilon}u^h + \lambda F(c, I)\right), \eta_i - u^h \rangle - \epsilon \langle \nabla u^h, \nabla(\eta_i - u^h) \rangle \geq 0 \quad \eta_i \in \mathcal{V}^{N,j},$$

an SSC method applied to this case consists of simply solving all such $\mathcal{P}_{i,j}$ by looping through all nodes i and levels j and updating the solution at each step, in whatever appropriate sequence the specific method demands.

Consider the finite element discretisation in (16); we firstly discretise in time using a backward Euler scheme to obtain the fully discrete problem. At each time step, j , we use the SSC method to efficiently update the approximation u^k as follows: starting at the coarsest level and moving to the finest in a standard multigrid w pattern, for every basis function η_L^i , $i = 1, 2, \dots, n_L$ on level L we update $u^{k+1} = u^k + \alpha_L^i$ where α_L^i satisfies the inequality

$$\hat{M}\left(\frac{u^k + \alpha_L^i \eta - u^j}{\delta t} + T\left(-\frac{2}{\epsilon}u^j + \lambda F(c^j, I)\right)\right) - \epsilon A(u^k + \alpha \eta) \geq 0$$

Once all basis functions and levels have been looped over, the iteration is complete; if the solution satisfies some prescribed error tolerance, it is accepted and becomes the new iterate u^{j+1} ; otherwise, the iteration is repeated using the computed iteration as the new starting point.

All basis functions η of all multigrid levels are projected onto the finest grid. An example of this projection is given in figure 2. Thus each iteration is of the form

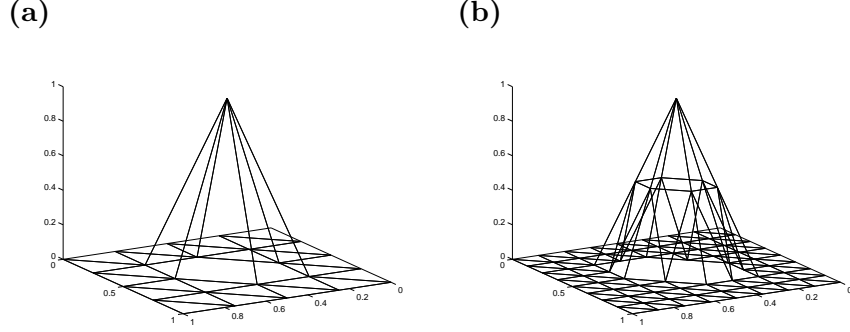


Fig. 2. a) A basis function defined on a coarse grid; b) the same basis function projected onto a finer grid

$$\hat{M} \left(\frac{u^k + \alpha\eta - u^t}{\delta t} + T \left(-\frac{2}{\epsilon} u^t + \lambda F(c^t, I) \right) \right) - \epsilon A(u^k + \alpha\eta) = 0$$

before projection into the required function space. It is enough to multiply both sides by η^T and re-arrange the above by simple algebra to obtain an equation for α :

$$\alpha \eta^T (\hat{M} - \epsilon \delta t A) \eta = \eta^T \left\{ \hat{M} \left[u^t - u^k + \delta t T \left(\frac{2}{\epsilon} u^t - \lambda F(c^t, I) \right) \right] + \epsilon A u^k \right\}. \quad (17)$$

C. Gibbs Space Constraint Pseudocode

In the vector-valued case, since N functions need to be updated simultaneously for each basis function, it is clear that α is also vector-valued and of size N . In order to preserve the constraint

$$\sum_{i=1}^N u_i = 1.$$

it must be that for each update

$$\sum_{i=1}^N \alpha_i = 0.$$

This is actually taken care of by the choice of minimisation, i.e. by involving the projection operator T and only allowing search directions $u + \alpha T v$.

Secondly, for the functions to remain in the Gibbs space \mathbb{G}^N at all times, at each iteration of the numerical scheme we must ensure that the result still lies in \mathbb{G}^N , i.e. in addition to the restriction on the sum of α above, all components of u must be positive. This requirement may be less than straightforward to enforce on coarse grids, where several nodes are affected by the change in α ; this is also mentioned in Kornhuber [17] and is due to the large support of the coarse grid basis functions after projection onto the finest grid; for that reason, a truncated multigrid algorithm may be more efficient than a full v-cycle.

The pseudo-code for a general subspace correction is given below; it is assumed that for each basis function, a list of affected nodes has been drawn so that the least amount of work possible is being done.

- 1) Evaluate α as per (17); then, calculate a trial version of u .
- 2) Check for each function u_i whether any of its entries have become negative. If not, no further work is required.

- 3) Otherwise, we have a split of the functions u_i into two sets, \mathbb{Q} being the set of u_i with negative (unacceptable) values, and \mathbb{P} being the remainder.

For each function in \mathbb{Q} , we need to determine a new α_i such that u_i remains between 0 and 1, i.e. such that the lowest value is zero. This is easily done and we refer to this correction as β . Since we know that $\sum \alpha = 0$ must be satisfied, if we decrease α_i then we need to increase all other $\alpha_j, j \neq i$ by a corresponding amount. However, we can exclude those functions that are already negative. Therefore, if there are k functions in \mathbb{P} and we decrease α_i by an amount β , then we need to decrease all α_k by β/k .

Do this for each function in \mathbb{Q} .

- 4) All functions in \mathbb{Q} are now guaranteed to lie between 0 and 1. However, the successive corrections β applied to the functions in \mathbb{P} may have caused some of those to become negative; hence, repeat from step 2, but only considering a restricted set of functions. Repeat this process until there are no more negative functions.

Since at least one function is being removed from the set of all available functions at each repetition of this process, it is a procedure of maximum order N complexity.

IV. IMPLEMENTATION

A. Determination of Natural Scales

In principle, it is necessary to consider the possibility that the interface between two areas of interest be only one pixel wide; in other words, that two neighbouring pixels belong to different objects in the image. It is well known that the interface width of the double obstacle Allen-Cahn equation is of $\mathcal{O}(\epsilon)$ - see for example [10] and references therein. This immediately suggests a natural length scale for the problem: an ϵ smaller than the size of a pixel in the given data would not make sense, and a larger ϵ would only blur edges and corners. All our computations have been performed using this natural length scale.

The value of ϵ also suggests an estimate for a plausible λ ; if the value $\sigma = \lambda\epsilon$ were much less than 1, the effects of the fidelity terms would be negligible; conversely, if it were too much larger than 1, the interface width would be reduced to such a slim margin that it could no longer be considered a diffuse interface. It was found in our computations that a value of roughly $\sigma \in [10, 100]$ gave the most interesting results.

However, it must be noted that the numerical discretisation of the Allen-Cahn equation can only give interface motion results of a satisfactory level of accuracy when there are several nodes to represent each interface, ideally 8 but in practice at least 4. In the context of a multigrid simulation, this can be achieved quite naturally by taking the given image's pixel structure as the reference grid and refining it an appropriate number of times - assuming uniform refinement to be the simplest case, where the number of nodes roughly doubles each time, this implies at least three refinements. It is also possible to coarsen the regular pixel grid a few times, depending on the size of the image. Thus the coarsest grid in the final setup will probably not correspond to the grid on which the data was defined.

Another consequence of the need for a refinement process is the need to represent the image data on a finer grid than the one it was defined on. In the present model, the only link between the evolution of the function u to the image to be processed are the fidelity terms of the form

$$\int_{\Omega} (I - c)^2 dx$$

with the constants

$$c = \frac{\int_{\Omega} Iu}{\int_{\Omega} u}$$

approximating the average of I on $\text{supp } u$. The method of implementation of these terms is therefore critical to obtaining a good result. Moreover, a decision needs to be made as to what function space the image I is assumed to belong to. There are several candidates, such as $C^\infty(\Omega)$ smooth functions, which make the mathematical analysis much easier and are generally derived by convolving the image data with a Gaussian; Lipschitz continuous functions, which include piecewise linear interpolants; and functions of bounded variation. This distinction can be of great practical importance to a finite element method because depending on the chosen approach to node placement and fidelity term implementation it may be necessary to compare the values of u and I at points that do not correspond to given pixel values, or to points that lie exactly on the boundary between two or more pixels (e.g. corners). Which space the image belongs to ultimately depends on what kind of data one is examining, but in this case we have chosen to consider the image as a set of piecewise constant values over each pixel; this is done in order not to artificially blur any edges before any computations have even taken place.

Together with mesh refinement, it is necessary to project the values of the original pixels to the fine grid. This is not done by interpolating the data values in any way, in order not to create spurious gradients. This is necessary because the fitting terms in our method rely on calculating the average value of I in each region; introducing new gradients also introduces small areas of different average value, which may be erroneously identified as new objects. Therefore, every newly created node is assigned exactly the same value as one of its neighbours. This preserves sharp discontinuities; it also leads to some staircasing of the data, but only on a relatively small scale that should be locked out by fixing ϵ on the coarse grid.

B. Data Projection

If it is indeed necessary to project the values of the original pixels to the fine grid, this should not be by interpolating the data values in any way, in order not to create spurious gradients. This is necessary because the fitting terms rely on calculating the average value of I in each region; introducing new gradients also introduces small areas of different average value, which may be erroneously identified as new objects in their own right. Therefore, every newly created node is assigned exactly the same value as one of its neighbours, which preserves sharp discontinuities. In other words, the image data is taken to represent an underlying function $I \in BV$ of bounded variation.

There are at least two distinct options for the implementation of these terms using a finite element model. The first is direct projection of the image data, node by node. The second is to note that the image function I is only weakly represented in the FE system, in the sense that only the value of its integral over a region is contained in the fidelity terms, and therefore in principle only the value of its integral on each element is required; projection can therefore be carried out triangle by triangle. This makes perfect sense as long as the triangulation is nested. In other words, the fidelity terms can be computed by either of the two following methods: either one uses the standard mass matrix,

$$M_{ij} = \langle \eta_i, \eta_j \rangle,$$

$$F = \sum_{n=1}^N M_{in} \cdot \left(I_n - \frac{M \cdot I \cdot u}{\sum M \cdot u} \right)^2$$

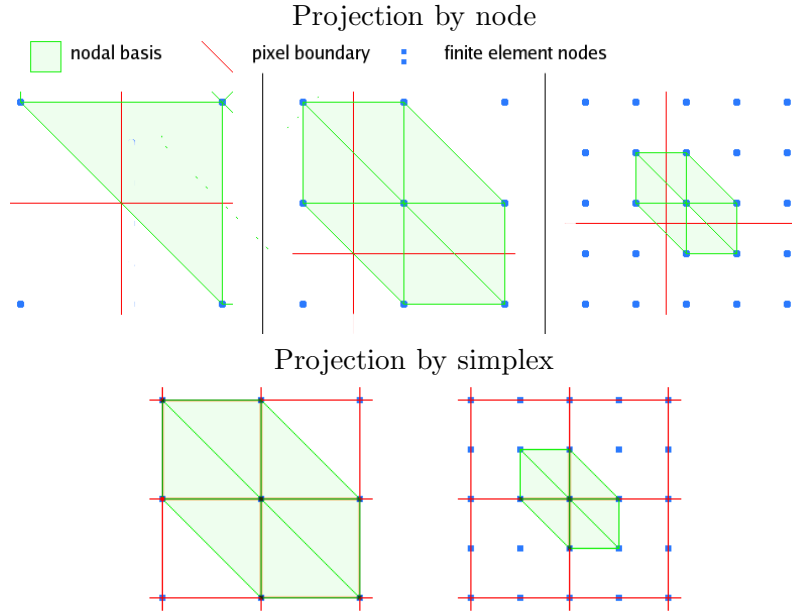


Fig. 3. A clarification of two different data projection schemes

or one computes the integral of I from first principles:

$$MI = \sum_{n=1}^N \sum_{t=1}^{\tau_n} I_t \langle \eta_i | t, \eta_n | t \rangle;$$

$$F = \left(MI - \frac{MI \cdot u}{\sum M \cdot u} \right)^2$$

Each method is associated with its own advantages, disadvantages, and computational costs. It is worth noting that the errors associated with each one decrease with each mesh refinement. The former can be thought of as *projection by node* and the latter as *projection by simplex*; examples are shown in figure 3.

C. Post-processing

Fig. 4a shows an example of the post-processed solution. The green and blue functions indicate segmented regions as identified by the program; using these, the average of the data, $osc I$, is used in each to obtain the denoised data (red). This process is easily achieved by multiplying said average by the component itself, then summing all the resulting components; this is referred to as the *composite*. Recall that the measure of $osc I$ on the support of each component u_i is already known and used actively in the fitting terms driving the evolution (see (5)). Further, because each component has values not identical to 0 or 1, notably at each interface, it is useful to round all values to either extremum, in such a way that only one component is equal to 1 and all others are 0 at any given point; in this way, segmented regions are defined more precisely. This naturally leads to the *rounded composite*, the advantage of which is shown in 4b, a comparison of the errors given by the composite and rounded composite.

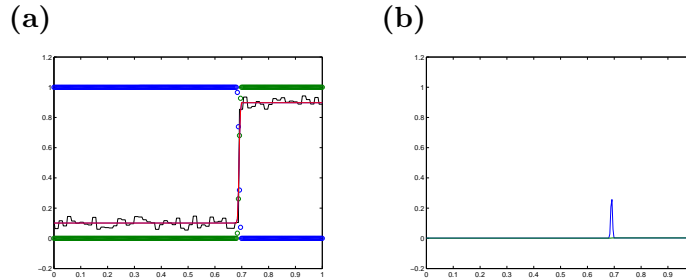


Fig. 4. a) A comparison of noisy data (black), segmented regions (green and blue), and resulting denoised signal (red); b) errors for the composite (blue) and rounded composite (green) segmentation.

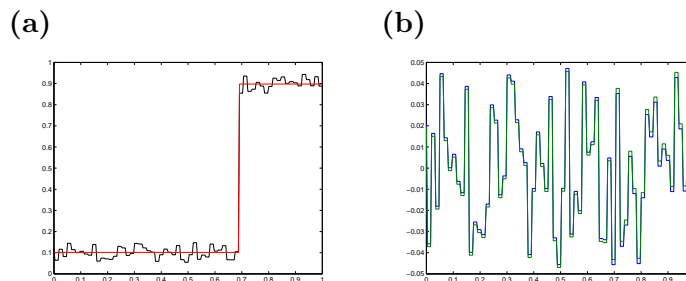


Fig. 5. a) noisy data (black) and rounded composite (red); b) original noise (blue) vs. recovered noise (green).

Figure 5a shows the noisy data (black) and the resulting rounded composite (red); for comparison, Fig. 5b shows the original noise (blue) and the recovered noise (green) obtained by subtracting the rounded composite from the initial data.

D. Two Dimensional Examples

Figure 6 shows the results of our method as applied to an image of concentric circles, with some noise. Figure 7 shows a more interesting case depicting what appears to be several overlapping geometric solids superimposed on a chequered background, for comparison with the results in Jung, Kang and Shen [14].

We also wish to examine the case of multi-channel data, the most obvious example of which is that of colour images. Although there is no reason why the proposed method could not be extended to images acquired at different wavelengths, for example by combining a visible night-time photograph with an infrared scan of the same area, the following arguments will concentrate on the case of colour images captured in the visible spectrum.

It may seem natural to perform the processing on each channel individually. However, this does not take into account the fact that the information gathered from each channel is not disjoint but has a certain, possibly stronger, correlation across channels rather than within the space of each channel - in other words, the same pixel on each channel most likely corresponds to the same object being photographed, whereas there's no such guarantee for any two adjacent pixels in the same

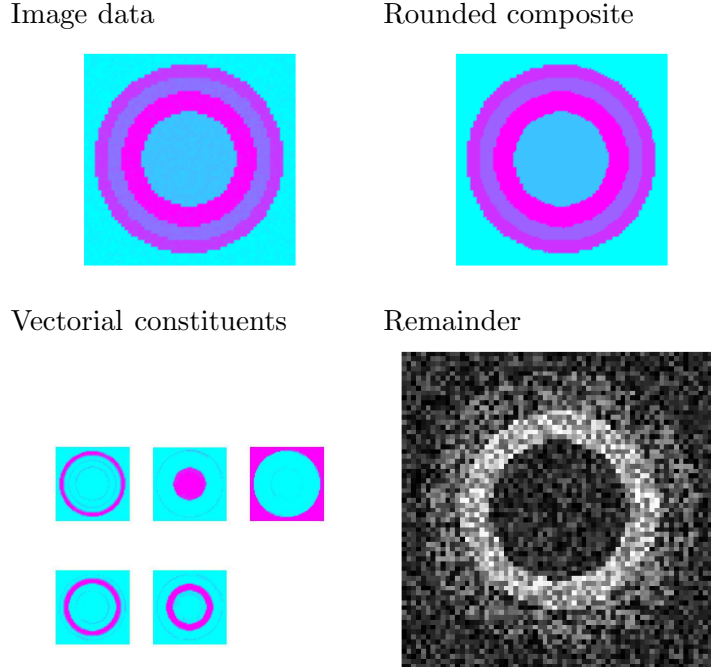


Fig. 6. Segmentation of four concentric circles at $[\.25 \ .95 \ .55 \ .75]$ over a background at level $.1$, with added random noise of amplitude $.05$. The remainder shows a combination of error and noise, scaled to show all detail

channel.² Also, the problem remains of how to combine the resulting information, and this is not a straightforward course of action in the case of segmentation.

Several methods to non-trivially process a colour image have previously been examined. The structure-texture decomposition method suggested by Meyer [23] was recently extended to colour images by Aujol and Kang [2] applying the G-norm to the RGB space. Another interesting approach is presented for example in Tang, Sapiro and Caselles [28], where the chromaticity values of each pixel are mapped onto the unit sphere and then processed using a diffusion-based filter; the authors consider both isotropic and anisotropic types. A rather similar approach seems to have been used in Yu and Bajaj [32], developed seemingly independently. It was argued in Kang and Shen [4] that a chromaticity-brightness (CB) filter outperforms a hue-saturation-value (HSV) filter in combination with a total variation method.

We propose to use multi-channel information in our model by adapting the fitting terms in (5) to use the information from each of the colour channels I_j :

$$c_{i,j}(u_i, I_j) = \frac{\int_{\Omega} u_i I_j}{\int_{\Omega} u_i}$$

²This depends on the field of interest. For example, in astronomy it may well be the case that a channel of information corresponds to a specific wavelength of light, in which case it is not only true that any one object is highly unlikely to appear across all wavelenghts, but the same absorption spectrum across different wavelenghts being captured at the same pixel most likely indicates two similar objects (e.g. gas clouds), one behind the other.

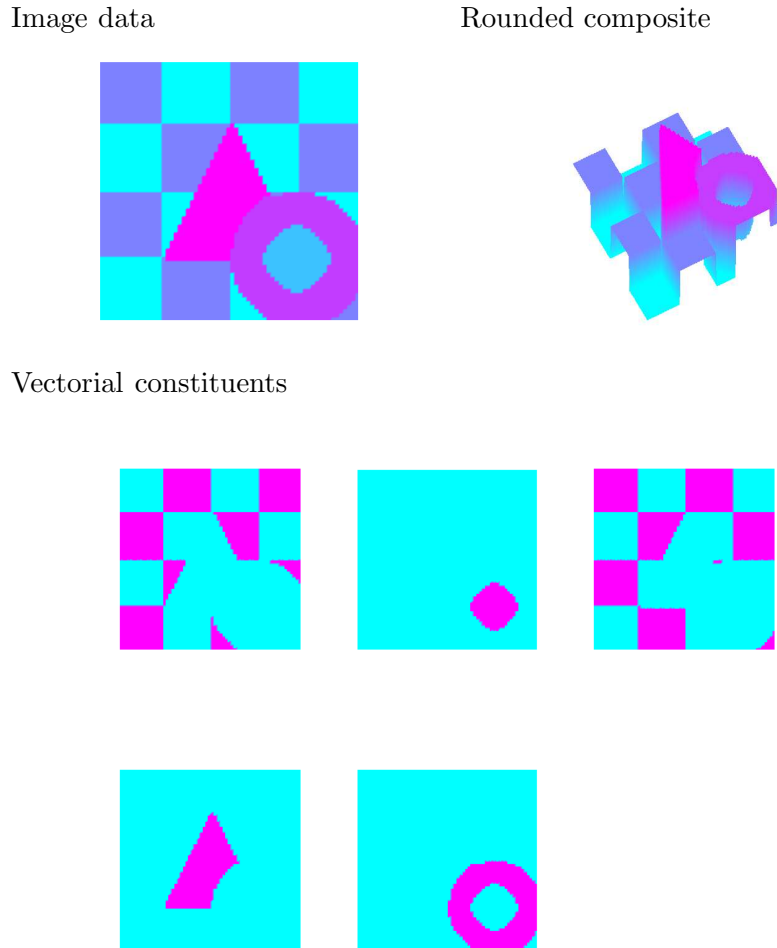


Fig. 7. Segmentation of a geometric composite

$$F(c_{i,j}, I_j) = \sum_{j=1}^3 |I_j - c_{i,j}(u_i, I_j)|^2 dx$$

This method can be followed regardless of how the multi-channel information is encoded, i.e. it can in principle be applied to any colour space, and any number of channels. For simplicity, the RGB space has been used in computations so far. Figures 8 and 9 were obtained using the RGB space. As can clearly be seen, the use of the RGB space cannot distinguish between a difference in colour and one in luminosity, potentially leading to somewhat unrealistic segmentations of complex real-world images; this could possibly be remedied by using the L*a*b* space and ignoring the luminosity component.

V. CONCLUSION

The method here presented is a flexible method for image segmentation and denoising based on the combination of previously consolidated work. It can either be fine-tuned to specific goals

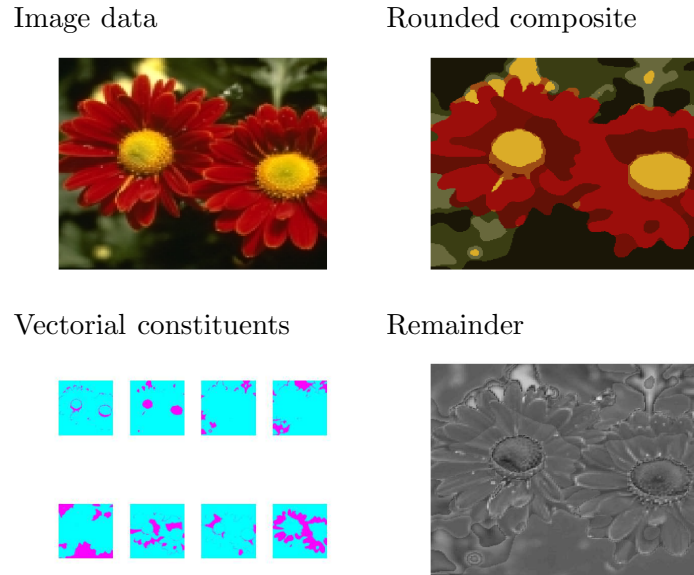


Fig. 8. Flowers



Fig. 9. Lena

or be allowed to run with almost no user input other than the initial image, which can define its own natural scale. Thanks to the multigrid formulation, computational costs will not spiral out of control. The method can also be further extended in several directions, including adaptive mesh refinement and adaptive time-stepping to further reduce computational time; it can deal with any desired colour space and any number of input and output channels, independent of each other.

The Esedoğlu-Tsai formulation involving MBO thresholding has the advantage of dealing well with the well-known unstable equilibrium value of $1/2$; however, we would suggest that there are important dynamics motivated by the Chan-Vese fitting terms, especially at short time-scales, that are lost by the thresholding mechanism. Our multigrid solution seeks to retain the computational swiftness while capturing the full dynamics of the equations.

REFERENCES

- [1] S. M. Allen and J. W. Cahn. A macroscopic theory for antiphase boundary motion and its applications to antiphase domain coarsening. *Acta Metal.*, 27:1085–1095, 1979.
- [2] J.-F. Aujol and S. H. Kang. Color image decomposition and restoration. *Journal of Visual Communication and Image Representation*, 17(4):916–928, August 2006. Previously appeared as UCLA CAM Report 04-73, December 2004.
- [3] M. Beneš, V. Chaloupecký, and K. Mikula. Geometrical image segmentation by the Allen-Cahn equation. *Applied Numerical Mathematics*, 51(2-3):187–205, 2004.
- [4] T. F. Chan, S.-H. Kang, and J. J. Shen. Total variation denoising and enhancement of color images based on the CB and HSV color models. *Journal of Visual Communication and Image Representation*, 12(4):422–435, 2001. Previously appeared as Tech. Report UCLA CAM 00-25, June 2001.
- [5] T. F. Chan, J. J. Shen, and L. Vese. Variational PDE models in image processing. *Notices of the American Mathematical Society*, 50(1):14–26, September 2002. Later appeared as Tech. Report UCLA CAM 02-61, December 2002.
- [6] T. F. Chan and L. Vese. An active contour model without edges. *Lecture Notes in Computer Science*, 1682:141–151, 1999.
- [7] T. F. Chan and L. Vese. Image segmentation using level sets and the piecewise-constant Mumford-Shah model. Technical Report 00-14, UCLA CAM, April 2000. Submitted to IJCV, 2000.
- [8] T. F. Chan and L. Vese. Active contours without edges. *IEEE Transactions on Image Processing*, 10(2):266–277, 2001. Previously appeared as Tech. Report UCLA CAM Report 98-53, December 1998.
- [9] T. F. Chan and L. Vese. A level set algorithm for minimizing the Mumford-Shah functional in image processing. In *IEEE/Computer Society Proceedings of the 1st IEEE Workshop on "Variational and Level Set Methods in Computer Vision"*, pages 161–168, 2001.
- [10] C. M. Elliott. Approximations of curvature dependent interface motion. In I. Duff and G. A. Watson., editors, *State of the Art Numerical Analysis*, pages 407–440. Clarendon Press, Oxford, 1997. Also appeared as University of Sussex, CMAIA Research Report 96/21.
- [11] S. Esedoğlu and Y.-H. R. Tsai. Threshold dynamics for the piecewise constant mumford-shah functional. *Journal of Computational Physics*, 211(1):367–384, 2006.
- [12] N. Fusco. An overview of the Mumford-Shah problem. *Milan Journal of Mathematics*, 71(1):95–119, September 2003.
- [13] H. Garcke, B. Nestler, and B. Stoth. On anisotropic order parameter models for multi-phase systems and their sharp interface limits. *Physica D*, 115:87–108, 1998.
- [14] Y. M. Jung, S. H. Kang, and J. Shen. Multiphase image segmentation via Modica-Mortola phase transition. Technical Report 06-31, UCLA CAM, June 2006.
- [15] R. Kornhuber. Monotone multigrid methods for elliptic variational inequalities I. *Numerische Mathematik*, 69:167–184, 1994.
- [16] R. Kornhuber. Nonlinear multigrid techniques. In J. Blowey, J. Coleman, and A. Craig, editors, *Theory and Numerics of Differential Equations*, pages 179–229. Springer Verlag, 2001.
- [17] R. Kornhuber. On multigrid methods for vector-valued Allen-Cahn equations with obstacle potential. In I. Herrera, D. E. Keyes, B. Olof, and R. Y. Widlund, editors, *Proceedings of the 14th international conference on Domain Decomposition Methods in Science and Engineering*, pages 307–314, 2003.
- [18] R. Kornhuber and R. Krause. On multigrid methods for vector-valued Allen-Cahn equations. In I. H. et al., editor, *Domain Decomposition Methods in Science and Engineering*, pages 307–314. UNAM, 2003.
- [19] R. Kornhuber and R. Krause. Robust multigrid methods for vector-valued Allen-Cahn equations with logarithmic free energy. *Computing and Visualization in Science*, 9(2):103–116, 2006.
- [20] J. Malik and P. Perona. Scale space and edge detection using anisotropic diffusion. *Proc. IEEE Computer Soc. Workshop on Computer Vision*, pages 6–22, 1987. Also appeared in *IEEE Transactions on Pattern Analysis and Machine Intelligence*, Vol. 12 no. 7 July 1990 pg 629–639.
- [21] B. Merriman, J. K. Bence, and S. J. Osher. Diffusion generated motion by mean curvature. Technical Report 92-18, UCLA CAM, April 1992.
- [22] B. Merriman, J. K. Bence, and S. J. Osher. Motion of multiple junctions: a level set approach. *Journal of Computational Physics*, 112(2):334–363, 1994.
- [23] Y. Meyer. Oscillating patterns in image processing and nonlinear evolution equations. In *The Fifteenth Dean Jacqueline B Lewis Memorial Lectures*, number 22 in University Lecture Series. AMS, 2001.
- [24] D. Mumford and J. Shah. Optimal approximation by piecewise smooth functions and associated variational problems. *Comm. Pure Appl. Math.*, 42:577–685, 1989.
- [25] N. Neuss. V-cycle convergence with unsymmetric smoothers and application to an anisotropic model problem. *SIAM Journal on Numerical Analysis*, 35(3):1201–1212, 1998.

- [26] J. Petitot. An introduction to the Mumford-Shah segmentation model. *Journal of Physiology - Paris*, 97:335–342, 2003.
- [27] X.-C. Tai and J. Xu. Global and uniform convergence of subspace correction methods for some convex optimization problems. *Mathematics of Computation*, 71(237):105–124, 2001.
- [28] B. Tang, G. Sapiro, and V. Caselles. Color image enhancement via chromaticity diffusion. *IEEE Transactions on Image Processing*, 10(5):701–707, May 2001.
- [29] L. A. Vese. Multiphase object detection and image segmentation. Technical Report 02-36, UCLA CAM, June 2002.
- [30] J. Xu. Iterative methods by space decomposition and subspace correction. *SIAM Review*, 34(4):581–613, 1992.
- [31] J. Xu. The method of subspace corrections. *Journal of Computational and Applied Mathematics*, 128:335–362, 2001.
- [32] Z. Yu and C. Bajaj. Anisotropic vector diffusion in image smoothing. In *Proceedings of International Conference on Image Processing*, pages 828–831, 2002.
- [33] H.-K. Zhao, T. Chan, B. Merriman, and S. Osher. A variational level set approach to multiphase motion. *J. Comput. Phys.*, 127(1):179–195, 1996.